Biochemistry and Biophysics Reports 17 (2019) 169–176

Contents lists available at ScienceDirect

Biochemistry and Biophysics Reports

journal homepage: www.elsevier.com/locate/bbrep

Involvement of the NADPH oxidase 2 pathway in renal oxidative stress in *Aqp11*$^{-/-}$ mice

Yuya Hoshino[a], Hiroko Sonoda[a], Ryuji Nishimura[a], Kazuya Mori[a], Kenichi Ishibashi[b], Masahiro Ikeda[a,*]

[a] Department of Veterinary Pharmacology, University of Miyazaki, Miyazaki 889-2192, Japan
[b] Department of Medical Physiology, Meiji Pharmaceutical University, Tokyo 204-8588, Japan

ARTICLE INFO

Keywords:
Aquaporin-11
Polycystic kidney disease
Oxidative stress
Hypoxia
Renal failure
Pathway analysis
NOX2

ABSTRACT

Aquaporin-11 (AQP11) is an intracellular AQP. Several studies with *Aqp11*$^{-/-}$ mice have shown that AQP11 has a role in normal development of the kidney after birth. Our previous studies have suggested that alteration of oxygen homeostasis may be involved in the kidney injury caused by AQP11 deficiency, although the underlying mechanism is largely unknown. To clarify this issue, we examined genes that are related to oxygen homeostasis in *Aqp11*$^{-/-}$ mice. Among 62 genes that are involved in oxygen homeostasis, 35 were upregulated by more than 2-fold in *Aqp11*$^{-/-}$ mice in comparison with wild-type mice. Pathway analysis using these genes extracted the pathway responsible for production of reactive oxygen species in macrophages. As expression of the genes involved in the NADPH oxidase 2 (NOX2) complex was dramatically increased by more than 14-fold, we further analyzed NOX2 at the protein level. Immunoblotting analysis demonstrated a dramatic increase of NOX2 protein in the kidney of *Aqp11*$^{-/-}$ mice, and immunohistochemistry showed that NOX2 protein and a marker protein for macrophages were increased in the renal interstitium. These results indicate that NOX2-induced oxidative stress accompanied by macrophage infiltration plays an important role in alteration of oxygen homeostasis in *Aqp11*$^{-/-}$ mice.

1. Introduction

Aquaporin-11 (AQP11), originally characterized by our group, is an integral membrane protein belonging to a larger family of major intrinsic proteins (MIP) [1]. It has been shown that AQP11 is localized at the endoplasmic reticulum (ER) and is permeable to water as well as glycerol [2–6]. A recent study has suggested that AQP11 plays a role in the maintenance of ER homeostasis [7]. Tissue distribution studies have revealed that AQP11 is well expressed in the kidney, testis, liver, and intestine [1,8,9].

In the kidney, AQP11 has been shown to be expressed in proximal tubule cells. Studies with *Aqp11*$^{-/-}$ mice have shown that loss of function of AQP11 seems to have no significant effect on renal physiology in the postpartum period, but thereafter causes ER vacuolization in proximal tubule cells following dilation of the proximal tubules, leading to the development of multiple renal cysts [1]. Most *Aqp11*$^{-/-}$ mice or AQP11 mutant mice (*Aqp11*$^{sjds/sjds}$) harboring a single amino acid substitution (Cys227Ser) die of renal failure by the age of 60 days [1,10].

Several previous studies have examined the mechanism by which AQP11 deficiency causes kidney injury. With regard to renal cyst formation in *Aqp11*$^{-/-}$ mice, Inoue et al. [11] have reported impairment of glycosylation processing and unusual membrane trafficking of polycystin-1, a protein encoded by the PKD1 gene whose mutation causes autosomal dominant polycystic kidney disease (ADPKD), the most common form of PKD in humans, suggesting that AQP11 deficiency induces cystogenesis through malfunction of polycystin-1. In addition to the mechanism of cystogenesis, several studies have examined the progression of kidney injury in *Aqp11*$^{-/-}$ mice. Studies of renal mRNAs have suggested that cell proliferation, remodeling of the extracellular matrix, apoptosis, and ER stress are possibly involved in the pathogenesis of the kidney injury [12]. Analytical studies of proteins in *Aqp11*$^{-/-}$ mice have shown that decreased levels of mitochondrial proteins are likely associated with kidney injury due to AQP11 deficiency [13]. Previously, our group has demonstrated that in *Aqp11*$^{sjds/sjds}$ mice the renal level of superoxide was increased and that an antioxidant ameliorated the reactive oxygen species (ROS)-related kidney injury in *Aqp11*$^{sjds/+}$ mice [14]. These data suggest that the mechanism of progression of kidney injury in *Aqp11*$^{-/-}$ mice involves an alteration of

* Correspondence to: Department of Veterinary Pharmacology, Faculty of Agriculture, University of Miyazaki, Gakuenkibanadai-Nishi 1-1, Miyazaki 889-2192, Japan.
E-mail address: a0d302u@cc.miyazaki-u.ac.jp (M. Ikeda).

https://doi.org/10.1016/j.bbrep.2019.01.003
Received 4 September 2018; Received in revised form 12 December 2018; Accepted 3 January 2019
Available online 11 January 2019

oxygen homeostasis, leading to apoptosis. However, the molecular mechanism operating in the pathway is largely unknown.

In the present study, in order to explore the molecular pathways involved in the progression of kidney injury in *Aqp11*$^{-/-}$ mice, we analyzed the mRNAs for genes involved in oxidative stress and hypoxia in these mice, and performed pathway analysis using the mRNA data. Our results suggest that aberrant oxygen homeostasis induced by increased expression of the renal NADPH oxidase 2 (NOX2) complex is involved in progression of the kidney injury caused by AQP11 deficiency.

2. Materials and methods

2.1. Animals and measurement of blood biochemistry

All animal studies were conducted according to the guidelines of the Care and Use of Laboratory Animals at the University of Miyazaki. As described previously, *Aqp11*$^{+/-}$ mice were interbred to obtain *Aqp11*$^{-/-}$ and wild-type (WT) littermates. Genotyping was performed by PCR as reported previously [1].

Kidney and blood samples were collected from 4-week-old male and female *Aqp11*$^{-/-}$ and from WT litters. Kidney samples from 12 mice (WT: n = 6, *Aqp11*$^{-/-}$: n = 6) were used for real-time PCR and those from 6 mice (WT: n = 3, *Aqp11*$^{-/-}$: n = 3) were used for a PCR array analysis. Blood was heparinized and separated into plasma by centrifugation. The concentrations of plasma creatinine and urea nitrogen were determined using an autoanalyzer (DRI-CHEM 3500i, Fuji Film, Tokyo, Japan).

2.2. RNA analyses

Total RNA was extracted from the right kidney using an RNeasy Protect Mini Kit (QIAGEN, Hilden, Germany) according to the manufacturer's protocol. The concentration of total RNA was measured using a spectrophotometer (ND-1000, Thermo Fisher Scientific, Waltham, MA).

Reverse-transcription of RNA was performed to produce cDNA using an iScript™ cDNA Synthesis Kit (Bio-Rad Laboratories, Hercules, CA, USA). For oxidative stress, we examined 15 genes involved in the production or elimination of ROS using real-time PCR (LightCycler® 96 System, Roche Diagnostics, Tokyo, Japan) and primers that are shown in Table 1. Data were normalized relative to the housekeeping gene *Tfrc*. We also analyzed genes related to hypoxia using TaqMan® Custom Arrays (P/N 4342253, Applied Biosystems, Foster City, CA), which includes 47 genes. The amplification reaction was performed using a 7900HT Fast Real-Time PCR System (Applied Biosystems). Data were normalized relative to the housekeeping gene 18S ribosomal RNA.

In the preliminary experiments, for validation of the internal controls such as *Tfrc* and 18S ribosomal RNAs, the ct values for each gene in *Aqp11*$^{-/-}$ and WT mice were compared. Consequently, the mean ± standard error of the mean (SEM) values were 13.15 ± 0.25 (WT mice for 18S ribosomal RNA, n = 3), 13.46 ± 0.25 (*Aqp11*$^{-/-}$ mice for 18 S ribosomal RNA, n = 3), 23.86 ± 0.63 (WT mice for *Tfrc* RNA, n = 3), and 23.75 ± 0.18 (*Aqp11*$^{-/-}$ mice for *Tfrc* RNA, n = 3), indicating that each gene was appropriate as an internal control.

2.3. Pathway analysis using mRNA expression data

Pathway analysis was performed to clarify the significant canonical pathway in the kidney of the *Aqp11*$^{-/-}$ mouse using Ingenuity® Pathway Analysis (IPA) (QIAGEN, www.qiagen.com/ingenuity). Genes whose expression in the kidney was changed by more than 2-fold in *Aqp11*$^{-/-}$ mice in comparison with WT mice were used for IPA analysis. The genes were mapped into canonical pathways based on the Ingenuity® Knowledge Base. In each canonical pathway, the p-value was calculated using Fisher's exact test.

2.4. Protein analyses

Left kidneys were homogenized in a homogenization solution composed of 300 mM sucrose, 25 mM imidazole, 1.3 mM EDTA, and complete protease inhibitor cocktail (Roche Diagnostics). The supernatant after centrifugation at 1,000*g* was then centrifuged at 200,000*g* at 4 °C for 1 h. The pellet was dissolved in the homogenization solution, mixed with 4 × sample buffer (8% SDS, 50% glycerol, 250 mM Tris·HCl, 0.05% bromophenol blue, 200 mM DTT, pH 6.8), and incubated at 37 °C for 30 min. The protein concentration of a small amount (less than 2% of total volume) of each pellet solution before mixing with 4 × sample buffer was determined using the BCA Protein Assay Kit (Thermo Fisher Scientific).

The protein samples were separated by SDS-PAGE, and then transferred to polyvinylidene difluoride (PVDF) membranes. The following antibodies were used for detection of specific proteins: anti-NOX2 antibody (#sc-130543, Santa Cruz Biotechnology, Santa Cruz, CA, USA) or anti-α-tubulin antibody (#T5168, SIGMA-ALDRICH, St. Louis, MO, USA) for the primary antibody, and peroxidase-conjugated anti-mouse IgG antibody (#1858413, Thermo Fisher Scientific) for the secondary antibody. Protein carbonyl analysis was performed using a Protein carbonyls western blot detection kit (ROIK03, SHIMA Laboratories,

Table 1
Primers for real-time PCR.

Gene	Forward	Reverse
Cat	5′-ACATGGTCTGGGACTTCTGG-3′	5′-CAAGTTTTTGATGCCCTGGT-3′
Gpx3	5′-CCGGGGACAAGAGAAGTCTA-3′	5′-CCAGAATGACCAAGCCAAAT-3′
Gsta1	5′-TGTTGAAGAGCCATGGACAA-3′	5′-ATCCATGGGAGGCTTTCTCT-3′
Hmox1	5′-TAAGCTGGTGATGGCTTCCT-3′	5′-GTGCAAGGGATGATTTCCTG-3′
Keap1	5′-TGAGCCAGCAACTCTGTGAC-3′	5′-TTCCATGACCTTAGGGTGGA-3′
Nox2	5′-ATGCAGGAAAGGAACAATGC-3′	5′-CCACACAGGAAAACGCCTAT-3′
Nox4	5′-TCTGGGTGTGCAGAGACATC-3′	5′-GCCCAATGAAAAGTCTCGAA-3′
Nrf2	5′-TGGAGAACATTGTCGAGCTG-3′	5′-TGGGAGAGTAAGGCTTTCCA-3′
p22phox	5′-TGGACGTTTCACACAGTGGT-3′	5′-ACCGACAACAGGAAGTGGAG-3′
p40phox	5′-TGAAGACACAGGCAAAACCA-3′	5′-ACCATGAGTCCCACATCCTC-3′
p47phox	5′-AGAAGGCTGGGGAGGAGATA-3′	5′-GATTGTCCTTTGTGCCATCC-3′
p67phox	5′-TGGCCTACTTCCAGAGAGGA-3′	5′-GCCAACTGCTCTTCTGCTTT-3′
Sod1	5′-GAGACCTGGGCAATGTGACT-3′	5′-TTGTTTCTCATGGACCACCA-3′
Sod2	5′-CCAAAGGAGAGTTGCTGGAG-3′	5′-TAAGGCCTGTTGTTCCTTGC-3′
Sod3	5′-CATGTCAAATCCAGGGGAGT-3′	5′-ATGCGTGTCGCCTATCTTCT-3′
Tfrc	5′-GGATCAAGCCAGATCAGCAT-3′	5′-AGTGCAATAGCTGCAAAGCA-3′

Cat, catalase; *Gpx3*, glutathione peroxidase 3; *Gsta1*, glutathione S-transferase alpha 1; *Hmox1*, heme oxygenase 1; *Keap1*, kelch like ECH associated protein 1; *Nox2*, NADPH oxidase 2; *Nox4*, NADPH oxidase 4; *Nrf2*, nuclear factor, erythroid 2 like 2; *Sod1*, superoxide dismutase 1; *Sod2*, superoxide dismutase 2; *Sod3*, superoxide dismutase 3; *Tfrc*, transferrin receptor.

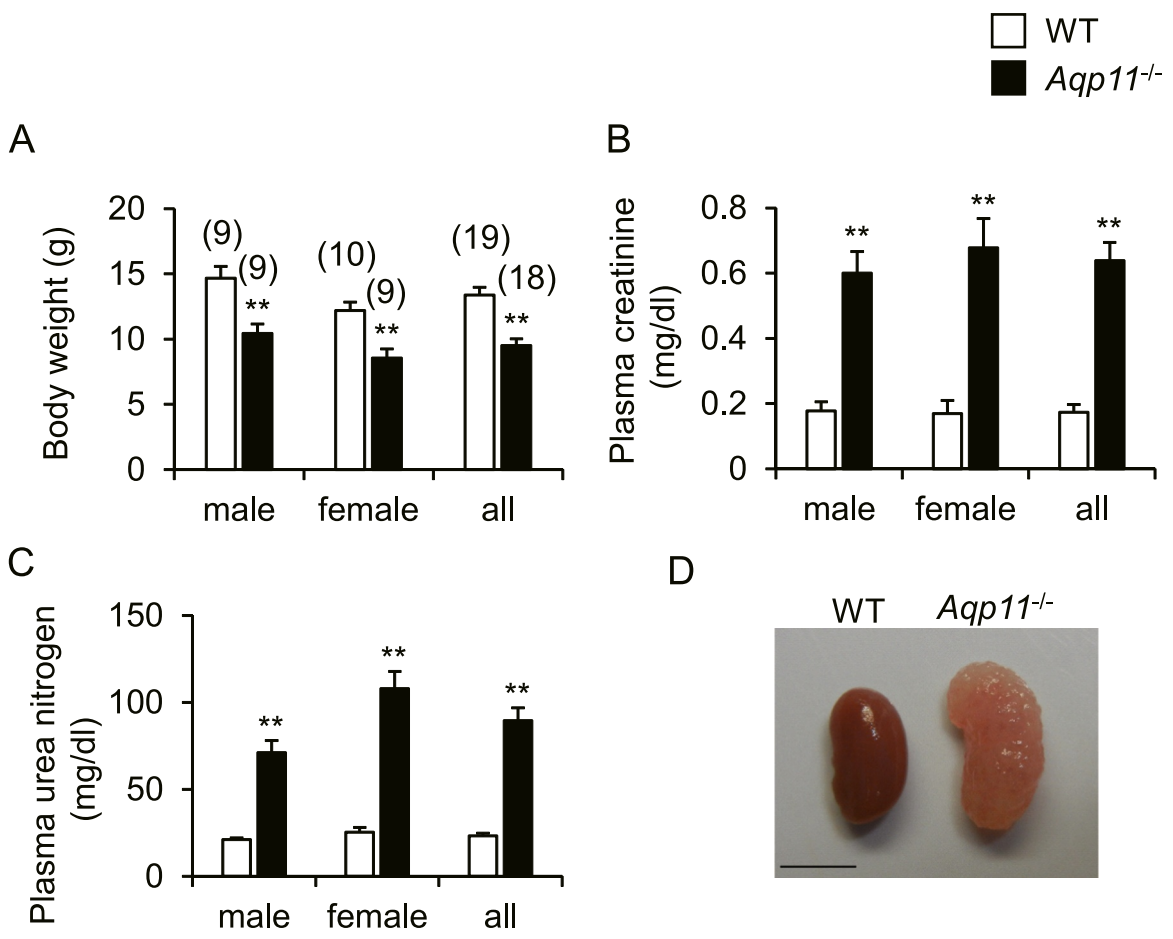

Fig. 1. Body weight, blood biochemistry and renal morphology in *Aqp11*$^{-/-}$ mice. A-C: Body weight (A), concentrations of plasma creatinine (B) and urea nitrogen (C) in males, females, and their combined data (all) for WT and *Aqp11*$^{-/-}$ mice. Numbers in parentheses indicate the number of animals tested. Values are expressed as means ± SEM. ** $P < 0.01$ compared with WT mice. D: Typical gross appearance of the kidney of female WT and *Aqp11*$^{-/-}$ mice. Scale bar: 5 mm.

Tokyo, Japan). In this experiment, peroxidase-conjugated anti-rabbit IgG antibody (#7074, Cell Signaling Technology, Danvers, MA, USA) was used as the secondary antibody. Bands were visualized using SuperSignal West Femto Maximum Sensitivity Substrate (Thermo Fisher Scientific). Band images were quantified using ImageQuant TL (GE Healthcare, Chicago, IL).

2.5. Histological analyses

A section (2 μm thick for serial sections and 3 μm thick for other sections) from a paraffin-embedded right kidney after antigen retrieval was reacted with anti-8-hydroxy-2′-deoxyguanosine (8-OHdG) antibody (#MOG-020P, JaICA, Shizuoka, Japan), anti-NOX2 antibody (#sc-130543, Santa Cruz Biotechnology) or anti-ionized calcium-binding adapter molecule 1 (IBA1) antibody (#PA527436, Thermo Fisher Scientific), followed by incubation with EnVision™ + Dual Link System-HRP (#K4063, DAKO Japan, Tokyo, Japan). Visualization of the antigen was performed with 3, 3′-diaminobenzidine tetrahydrochloride. Sections were counterstained with hematoxylin.

For terminal deoxynucleotidyl transferase dUTP nick end labeling (TUNEL) assay, a TdT-FragEL™ DNA Fragmentation Detection Kit (#QIA33, Merck, Darmstadt, Germany) was employed.

2.6. Statistical analysis

All data were expressed as means ± SEM. Comparisons between two groups were performed using Student's *t*-test. Differences at $P < 0.05$ were considered statistically significant.

3. Results

3.1. Basal characteristics of *Aqp11*$^{-/-}$ mice

Body weight, concentrations of plasma creatinine and urea nitrogen, and renal gross morphology in WT mice and *Aqp11*$^{-/-}$ mice are shown in Fig. 1. Body weight was significantly lower in *Aqp11*$^{-/-}$ mice than in WT mice (Fig. 1A). Concentrations of plasma creatinine and urea nitrogen were significantly higher in *Aqp11*$^{-/-}$ mice (Fig. 1B and C). Grossly, kidneys from *Aqp11*$^{-/-}$ mice were larger and paler than those from WT mice (Fig. 1D). These results indicated that renal failure occurred in *Aqp11*$^{-/-}$ mice as reported previously [1,10]. Because our data showed that the above parameters were similar between male and female *Aqp11*$^{-/-}$ mice, we used male mice for further analysis.

Previously we have reported that the level of renal superoxide was increased in AQP11 mutant mice relative to WT mice [14]. In this context, we investigated other markers of oxidative stress. We first checked the protein carbonyl content, an oxidative stress marker for protein. As shown in Fig. 2A and B, the protein carbonyl content of the kidney was increased in *Aqp11*$^{-/-}$ mice relative to WT mice.

Next, we examined the renal level of 8-OHdG, an oxidative stress marker for DNA, using immunohistochemistry. As shown in Fig. 2C and D, the number of 8-OHdG-positive cells was increased in the renal interstitium of *Aqp11*$^{-/-}$ mice, in comparison with WT mice. These results clearly indicated that oxidative stress was increased in the progressive phase of kidney injury in *Aqp11*$^{-/-}$ mice.

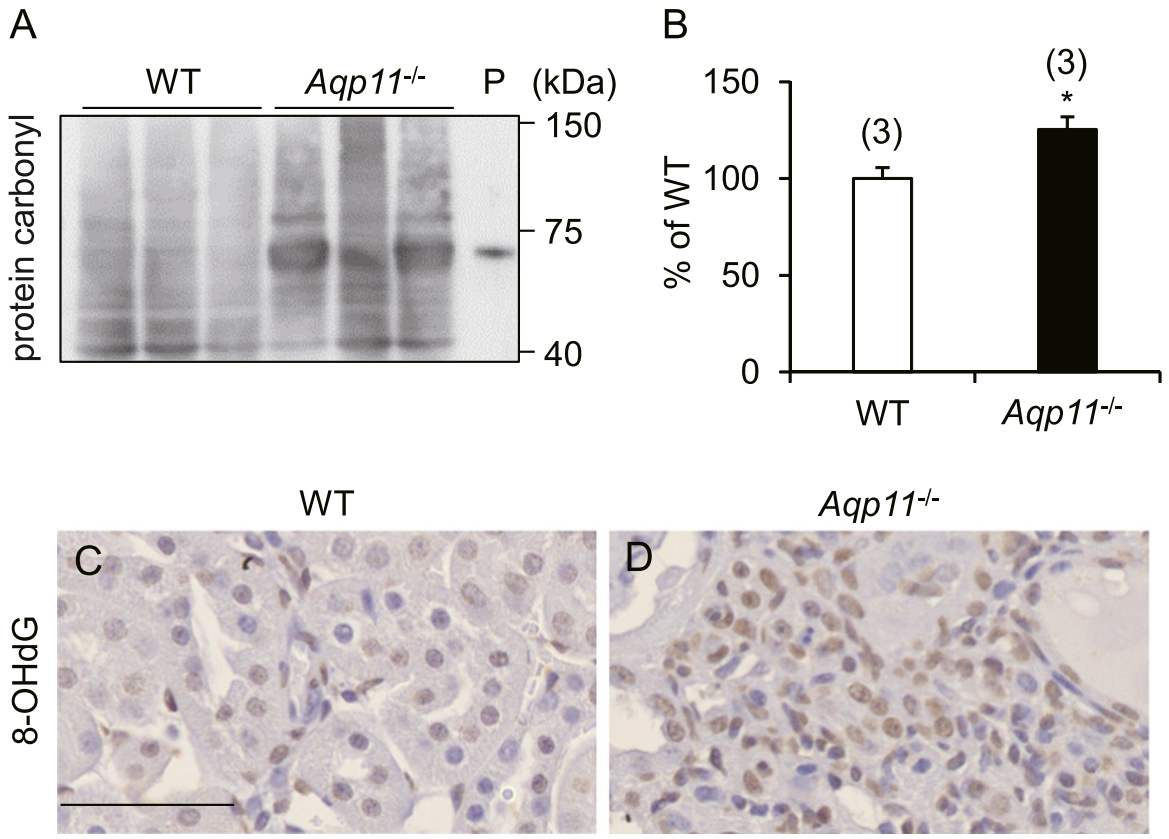

Fig. 2. Increased level of renal oxidative stress in *Aqp11*$^{-/-}$ mice. A-B: Immunoblot analysis of the renal protein carbonyl content in WT and *Aqp11*$^{-/-}$ mice. A: A typical immunoblot. The bands over a wide range indicate protein carbonyl. P: Positive control (oxidative bovine serum albumin). B: Quantitative analysis of renal protein carbonyl content. Numbers in parentheses indicate the number of animals tested. Values are expressed as percentages of the mean value in WT mice. * $P < 0.05$ compared with WT mice. C-D: Typical results of immunohistochemistry for renal 8-OHdG in WT (C) and *Aqp11*$^{-/-}$ (D) mice. Brown color indicates the presence of 8-OHdG. Scale bar: 50 μm.

3.2. Renal expression of mRNAs for genes involved in oxidative stress and hypoxia in *Aqp11*$^{-/-}$ mice

After confirmation of increased oxidative stress in the kidney of *Aqp11*$^{-/-}$ mice, we examined the renal expression of mRNAs for genes involved in oxygen homeostasis. As shown in Table 2, 35 out of 62 genes were up-regulated with a fold change higher than 2 in *Aqp11*$^{-/-}$ mice in comparison with WT mice. The top 10 genes included *p47phox* (fold change: 44.66), *p40phox* (33.17), *Nox2* (23.61), *p67phox* (14.97), *Edn1* (13.31), *Ednra* (11.49), *Col18a1* (7.04), *Hmox1* (5.69), *Notch1* (5.48), *Nrf2* (4.38).

3.3. Pathway analysis using renal mRNA expression data

In order to examine which molecular pathways were activated in the kidney of *Aqp11*$^{-/-}$ mice, we employed IPA using the results of mRNA analysis. Table 3 shows the top 15 canonical pathways with a *p* value lower than 5.75E-04, including the pathways related to oxygen homeostasis such as “Hypoxia Signaling in the Cardiovascular System”, “HIF1α Signaling”, “NRF2-mediated Oxidative Stress Response”, and “Production of Nitric Oxide and Reactive Oxygen Species in Macrophages”.

3.4. Renal expression of NOX2 protein and macrophage infiltration in *Aqp11*$^{-/-}$ mice

NOX2 is a member of the NADPH oxidase family which generates superoxide at biological membranes. NOX2 forms a complex composed of NOX2 protein, p22phox, Ras-related C3 botulinum toxin substrate (RAC), p40phox, p47phox and p67phox. As mentioned earlier, expression levels of *Nox2*, *p40phox*, *p47phox* and *p67phox* were dramatically up-regulated by a fold change of more than 14 in *Aqp11*$^{-/-}$ mice. Therefore, we further studied the kidney of *Aqp11*$^{-/-}$ mice, focusing on this molecular pathway. Immunoblot analysis showed that the expression of renal NOX2 protein was significantly increased in *Aqp11*$^{-/-}$ mice in comparison with WT mice (Fig. 3A and B). In addition, immunohistochemistry showed that the increase of NOX2 protein was mainly evident in the renal interstitial region of *Aqp11*$^{-/-}$ mice (Fig. 3E and G).

Since it has been reported that NOX2 is highly expressed in phagocytes such as monocytes and macrophages [15], we examined renal infiltration of macrophages in *Aqp11*$^{-/-}$ mice. Immunohistochemistry for IBA1, a marker protein for macrophages, with a serial section from the same block that had been used for the above-mentioned NOX2 protein staining, clearly showed that the number of IBA1-positive macrophages was markedly increased in the renal interstitium in *Aqp11*$^{-/-}$ mice (Fig. 3F and H) and that some macrophages appeared to co-express both NOX2 protein and IBA1 (arrowheads in Fig. 3G and H).

3.5. Apoptosis in the kidney of *Aqp11*$^{-/-}$ mice

As it is well known that enhanced oxidative stress causes apoptosis [16], we examined the number of apoptotic cells in the kidney of *Aqp11*$^{-/-}$ mice using the TUNEL assay (Fig. 4A-C). TUNEL-positive cells were significantly increased in the kidney of *Aqp11*$^{-/-}$ mice in comparison with WT mice and this increase was mainly observed in the renal interstitium and, to a lesser extent, the renal tubules such as the proximal tubules.

Table 2
Renal expression of mRNAs for genes related to oxidative stress or hypoxia in *Aqp11*$^{-/-}$ mice.

Gene	Fold change	*p* value	Gene	Fold change	p-value
Adm	2.88	0.014	*Hnf4a*	1.18	0.690
Agt	3.64	0.006	*Hyou1*	2.21	0.039
Angptl4	1.72	0.039	*Igfbp1*	− 1.95	0.241
App	1.85	0.084	*Ing4*	2.02	0.032
Arnt	3.06	0.013	*Keap1*	3.46	1.62E-04
Arnt2	3.34	0.023	*Mb*	ND	
Atp1b1	1.59	0.225	*Mtor*	1.72	0.145
Bhlhe40	4.14	0.026	*Nos1*	ND	
Birc2	2.90	0.102	*Nos3*	4.31	0.019
Camk2g	2.28	0.038	*Notch1*	5.48	0.010
Casp1	5.89	0.086	*Nox2*	23.61	0.008
Cat	− 1.07	0.699	*Nox4*	1.04	0.871
Col18a1	7.04	0.010	*Nrf2*	4.38	0.001
Ddit4l	2.53	0.011	*p22phox*	1.36	0.333
Dusp1	3.07	0.008	*p40phox*	33.17	0.019
Edn1	13.31	0.056	*p47phox*	44.66	0.028
Ednra	11.49	0.005	*p67phox*	14.97	0.009
Egf	− 1.75	0.405	*Pik3ca*	1.49	0.230
Egln1	1.73	0.102	*Plagl2*	4.60	0.017
Egln2	1.71	0.130	*Prl4a1*	ND	
Egln3	3.71	0.029	*Pten*	1.86	0.098
Ep300	2.40	0.054	*Rb1*	2.40	0.048
Epas1	2.89	0.020	*Sim1*	2.04	0.083
Epo	ND		*Sim2*	2.06	0.060
Erbb2	1.54	0.268	*Slc2a8*	1.79	0.081
Gpx3	1.04	0.880	*Sod1*	− 1.11	0.755
Gsta1	1.06	0.805	*Sod2*	− 1.08	0.700
Hif1a	2.66	0.013	*Sod3*	1.28	0.189
Hif1an	2.61	0.034	*Sp1*	2.32	0.071
Hif3a	ND		*Tgfbr2*	4.18	0.049
Hmox1	5.69	0.002	*Wt1*	1.08	0.874

ND: not detected.

4. Discussion

In a previous study, we observed that renal ROS production was increased and that sulforaphane, an antioxidant, ameliorated ROS-related kidney injury in AQP11 mutant mice [14]. However, the molecular mechanism of oxidative stress in the AQP11-deficient kidney has not yet been clarified. In the present study, oxidative stress was increased in the renal interstitium of *Aqp11*$^{-/-}$ mice. Along with this increase, the levels of *Nox2*, *p40phox*, *p47phox* and *p67phox* mRNAs were markedly upregulated in *Aqp11*$^{-/-}$ mice by more than 10-fold in comparison with WT mice. Also, increased expression of NOX2 protein was observed in the renal interstitium, possibly infiltrated macrophages. On the other hand, the levels of antioxidant enzyme genes such as *Cat*, *Gpx3*, and *Sod 1–3* were not significantly down-regulated in the kidney of *Aqp11*$^{-/-}$ mice relative to WT mice. These data suggested that the increased ROS production in the kidney of *Aqp11*$^{-/-}$ mice was mediated mainly by the NOX2 pathway of the infiltrated macrophages, and that reduction of anti-oxidant activity is minimal.

Oxidative stress is reportedly involved in the progression and poor outcome of ADPKD. Maser et al. [17] have observed that marker molecules for renal oxidative stress are increased in the kidneys of *cpk* mice and *Han:SPRD-cy* rats, both of which are animal models of ADPKD, accompanied by a reduction in the expression of renal antioxidant mRNAs and proteins, including GST-Ya, catalase, and MnSOD. In human ADPKD, Menon et al. [18] have observed both increased epi-PGF2α and decreased SOD levels in urine of patients with ADPKD in comparison with healthy controls. These data, together with our present results, indicate that increased oxidative damage is one important mechanism involved in the progression of PKD. However, reduction of antioxidants might play only a minimal role in the renal production of ROS in *Aqp11*$^{-/-}$ mice, in contrast to the results obtained in human ADPKD and animal models of ADPKD. The reason for this is currently unclear, and further investigation is required.

Macrophage infiltration of the renal interstitium in *Aqp11*$^{-/-}$ mice was observed in the present study. Several studies have demonstrated that macrophages play an important role in the progression of kidney injury in ADPKD; not only have they (CD68-positive cells) been detected in ADPKD patients [19], but an increased level of monocyte chemoattractant protein 1 (MCP1) has been demonstrated in the cystic fluid [20]. Interestingly, Karihaloo et al. [21] have described that cultured *Pkd1*-deficient cells expressed a higher level of MCP1 and augmented macrophage migration activity. These reports suggest that dysfunction of polycystin-1 causes MCP1-induced macrophage chemotaxis in ADPKD. Since it has been reported that deficiency of AQP11 causes mislocalization of polycystin-1, leading to its dysfunction [11], increased infiltration of macrophages into the kidneys of *Aqp11*$^{-/-}$ mice might be related to the dysfunction of polycystin-1 caused by loss of AQP11.

Our analyses of mRNA revealed that *Edn1* and *Ednra*, which encode endothelin and endothelin receptor type A, respectively, were markedly up-regulated in the kidneys of *Aqp11*$^{-/-}$ mice. Previous studies using transgenic mice showed that overexpression of endothelin-1 resulted in

Table 3
Top 15 canonical pathways.

Ingenuity Canonical Pathway	-log(*p* value)	Ratio	z-score	Molecules
Hypoxia Signaling in the Cardiovascular System	8.92	0.0811	1.000	ARNT, EDN1, EP300, HIF1AN, HIF1A, NOS3
HIF1α Signaling	7.64	0.0500	NC	ARNT, EDN1, EGLN3, EP300, HIF1A, NOS3
Osteoarthritis Pathway	7.55	0.0323	0.816	CASP1, EP300, EPAS1, HIF1A, NOTCH1, SP1, TGFBR2
Molecular Mechanisms of Cancer	5.87	0.0182	NC	BIRC2, CAMK2G, EP300, HIF1A, NOTCH1, RB1, TGFBR2
Aryl Hydrocarbon Receptor Signaling	5.61	0.0342	0.447	ARNT, EP300, NFE2L2 (NRF2), RB1, SP1
Xenobiotic Metabolism Signaling	5.39	0.0207	NC	ARNT, CAMK2G, EP300, HMOX1, KEAP1, NFE2L2 (NRF2)
Renal Cell Carcinoma Signaling	5.11	0.0471	NC	ARNT, EGLN3, EP300, HIF1A
Hepatic Fibrosis / Hepatic Stellate Cell Activation	5.09	0.0267	NC	AGT, COL18A1, EDN1, EDNRA, TGFBR2
Endothelin-1 Signaling	4.89	0.0244	2.236	CASP1, EDN1, EDNRA, HMOX1, NOS3
Pancreatic Adenocarcinoma Signaling	4.52	0.0333	NC	HMOX1, NOTCH1, RB1, TGFBR2
NRF2-mediated Oxidative Stress Response	3.72	0.0207	1.000	EP300, HMOX1, KEAP1, NFE2L2 (NRF2)
Production of Nitric Oxide and Reactive Oxygen Species in Macrophages	3.66	0.0200	2.000	CYBB (NOX2), NCF1 (p47phox), NCF2 (p67phox), NCF4 (p40phox)
Leukocyte Extravasation Signaling	3.52	0.0184	NC	CYBB (NOX2), NCF1 (p47phox), NCF2 (p67phox), NCF4 (p40phox)
Protein Kinase A Signaling	3.48	0.0123	1.342	CAMK2G, DUSP1, EP300, NOS3, TGFBR2
VEGF Signaling	3.24	0.0275	NC	ARNT, HIF1A, NOS3

Ratio, ratio of the number of molecules mapped into the canonical pathway in our mRNA dataset relative to the total number of molecules in the pathway; z-score, the value indicating whether any given pathway is activated or inhibited; Molecules, the molecules in our mRNA dataset which map to the canonical pathways; NC, not calculated.

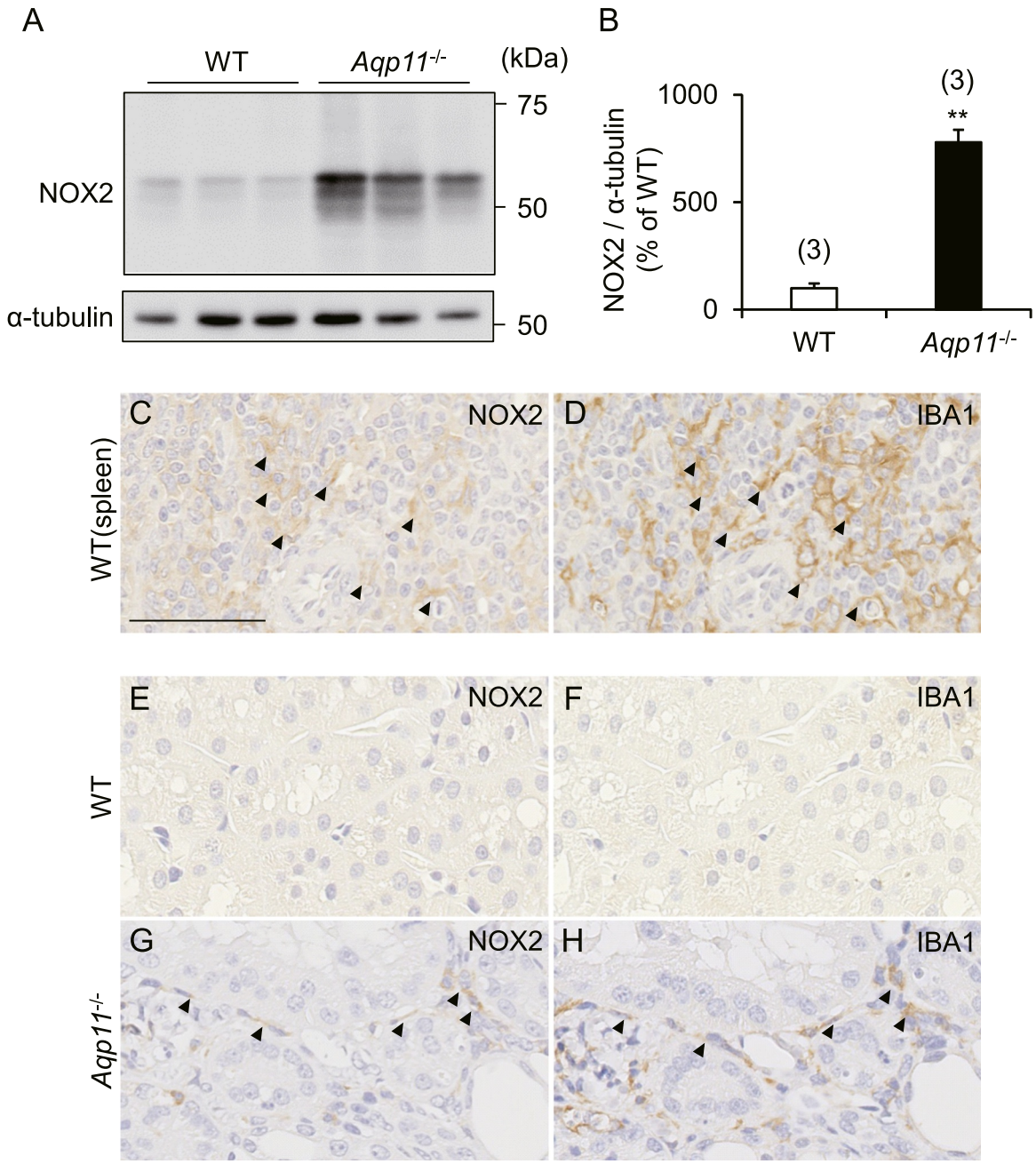

Fig. 3. Renal expression of NOX2 protein and macrophage infiltration in *Aqp11*$^{-/-}$ mice. A-B: Immunoblot analysis of NOX2 in WT and *Aqp11*$^{-/-}$ mice. A: Typical immunoblots. B: Quantitative analysis of renal expression levels of NOX2. Data are normalized by the level of α-tubulin. Numbers in parentheses indicate the number of animals tested. Values are expressed as percentages of the mean level in WT mice. ** $P < 0.01$ compared with WT mice. C-D: In order to confirm the specificities of the antibodies against NOX2 protein and IBA1 in the immunohistochemistry experiments, we checked the localization of NOX2 protein (C) and IBA1 (D) in serial sections from the same block of the spleen taken from WT mice, because the red pulp of the spleen has been reported to contain macrophages [30]. Typical results of immunohistochemistry are shown. Arrowheads indicate the possible co-localization of both proteins. E-H: Typical results of immunohistochemistry with serial sections for NOX2 protein (E & G) and IBA1 (F & H) in WT (E & F) and *Aqp11*$^{-/-}$ (G & H) mice. Arrowheads indicate the possible co-localization of both proteins. Scale bar: 50 μm.

formation of renal cysts and renal failure [22,23]. Increased expression of mRNAs for endothelin-1 and endothelin receptor type A has also been reported in the kidneys of *cpk* mice [24], and patients with ADPKD [25]. Therefore, it is possible that endothelin signaling may also be related to the pathobiology of kidney injury in *Aqp11*$^{-/-}$ mice.

Recently, it has been reported that human *AQP11* polymorphism with a single Gly102Ser amino acid substitution is related to the progression of type 2 diabetic nephropathy [26] and the outcome of the renal allograft in kidney transplantation [27]. On the other hand, NOX2-induced oxidative stress has been implicated in the pathology of diabetic nephropathy [28] and fibrosis in renal allografts [29]. Therefore, NOX2-induced oxidative stress caused by reduced function of AQP11 might be relevant to the pathology of diabetic nephropathy and renal allograft dysfunction.

In conclusion, we have demonstrated that the *Aqp11*$^{-/-}$ mouse shows alterations of renal oxygen homeostasis such as oxidative stress and hypoxia. In particular, oxidative stress induced by increased levels of NOX2 may play a significant role, leading to progression of renal impairment.

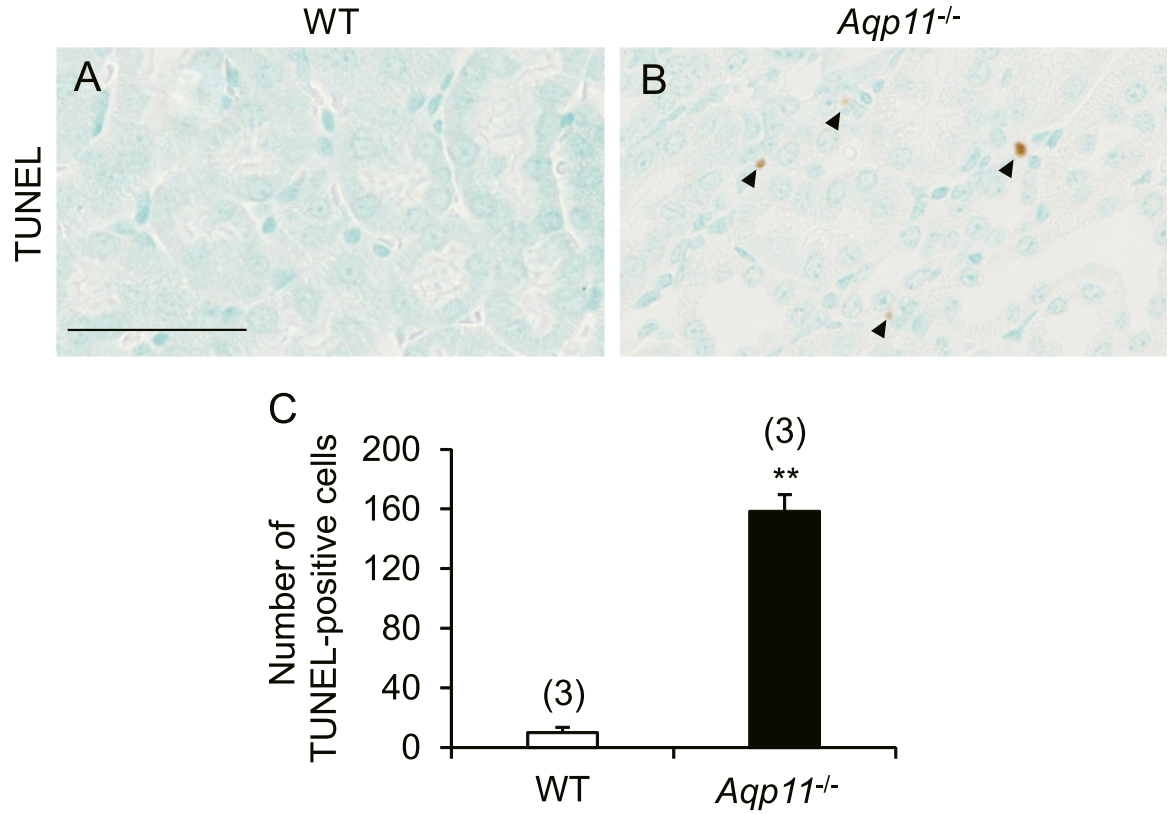

Fig. 4. Renal apoptosis in *Aqp11*$^{-/-}$ mice. A-B: Typical results of the TUNEL assay in kidney sections from WT (A) and *Aqp11*$^{-/-}$ (B) mice. Counterstaining was performed with methylene blue. Arrowheads indicate TUNEL-positive cells. Scale bar: 50 μm. C: The number of TUNEL-positive cells per whole kidney section in WT and *Aqp11*$^{-/-}$ mice was counted and the mean ± SEM from 3 animals for each group is shown. ** $P < 0.01$.

CRediT authorship contribution statement

Yuya Hoshino: Conceptualization, Data curation, Formal analysis, Investigation, Methodology, Writing - original draft, Writing - review & editing. **Hiroko Sonoda:** Formal analysis, Funding acquisition, Investigation, Methodology, Writing - original draft, Writing - review & editing. **Ryuji Nishimura:** Investigation, Methodology. **Kazuya Mori:** Investigation, Methodology. **Masahiro Ikeda:** Conceptualization, Data curation, Formal analysis, Funding acquisition, Investigation, Methodology, Project administration, Supervision, Writing - original draft, Writing - review & editing.

Acknowledgements

This work was supported by JSPS KAKENHI, 15H04594 (M.I.), 16K15047 (M.I.), 18H02348 (M.I.), 15K18784 (H.S.), and 18K05996 (H.S.).

Author contributions

Y.H., H.S., and M.I. designed the research; Y.H., H.S., R.N., K.M., and M.I. performed the research; Y.H., H.S., and M.I. analyzed the data; Y.H., H.S., and M.I. interpreted the results of experiments; Y.H., K.I. and M.I. wrote the manuscript.

Appendix A. Supporting information

Supplementary data associated with this article can be found in the online version at doi:10.1016/j.bbrep.2019.01.003.

References

[1] Y. Morishita, T. Matsuzaki, M. Hara-chikuma, A. Andoo, M. Shimono, A. Matsuki, K. Kobayashi, M. Ikeda, T. Yamamoto, A. Verkman, E. Kusano, S. Ookawara, K. Takata, S. Sasaki, K. Ishibashi, Disruption of aquaporin-11 produces polycystic kidneys following vacuolization of the proximal tubule, Mol. Cell Biol. 25 (2005) 7770–7779.

[2] M. Ikeda, A. Andoo, M. Shimono, N. Takamatsu, A. Taki, K. Muta, W. Matsushita, T. Uechi, T. Matsuzaki, N. Kenmochi, K. Takata, S. Sasaki, K. Ito, K. Ishibashi, The NPC motif of aquaporin-11, unlike the NPA motif of known aquaporins, is essential for full expression of molecular function, J. Biol. Chem. 286 (2011) 3342–3350.

[3] A. Madeira, S. Fernández-Veledo, M. Camps, A. Zorzano, T.F. Moura, V. Ceperuelo-Mallafré, J. Vendrell, G. Soveral, Human aquaporin-11 is a water and glycerol channel and localizes in the vicinity of lipid droplets in human adipocytes, Obesity 22 (2014) 2010–2017.

[4] S. Takahashi, K. Muta, H. Sonoda, A. Kato, A. Abdeen, M. Ikeda, The role of Cysteine 227 in subcellular localization, water permeability, and multimerization of aquaporin-11, FEBS Open Bio. 4 (2014) 315–320.

[5] K. Yakata, K. Tani, Y. Fujiyoshi, Water permeability and characterization of aquaporin-11, J. Struct. Biol. 174 (2011) 315–320.

[6] D.A. Gorelick, J. Praetorius, T. Tsunenari, S. Nielsen, P. Agre, Aquaporin-11: a channel protein lacking apparent transport function expressed in brain, BMC Biochem. 7 (2006) 14.

[7] A. Rojek, E.M. Füchtbauer, A. Füchtbauer, S. Jelen, A. Malmendal, R.A. Fenton, S. Nielsen, Liver-specific Aquaporin 11 knockout mice show rapid vacuolization of the rough endoplasmic reticulum in periportal hepatocytes after amino acid feeding, Am. J. Physiol. Gastrointest. Liver Physiol. 304 (2013) 501–515.

[8] C.H. Yeung, T.G. Cooper, Aquaporin AQP11 in the testis: molecular identity and association with the processing of residual cytoplasm of elongated spermatids, Reproduction 139 (2010) 209–216.

[9] C. Zhu, Z. Chen, Z. Jiang, Expression, distribution and role of aquaporin water channels in human and animal stomach and intestines, Int. J. Mol. Sci. 17 (2016) 1399.

[10] E.E. Tchekneva, Z. Khuchua, L.S. Davis, V. Kadkina, S.R. Dunn, S. Bachman, K. Ishibashi, E.M. Rinchik, R.C. Harris, M.M. Dikov, M.D. Breyer, Single amino acid substitution in aquaporin 11 causes renal failure, J. Am. Soc. Nephrol. 19 (2008) 1955–1964.

[11] Y. Inoue, E. Sohara, K. Kobayashi, M. Chiga, T. Rai, K. Ishibashi, S. Horie, X. Su, J. Zhou, S. Sasaki, S. Uchida, Aberrant glycosylation and localization of polycystin-1 cause polycystic kidney in an AQP11 knockout model, J. Am. Soc. Nephrol. 25 (2014) 2789–2799.

[12] S. Okada, T. Misaka, Y. Tanaka, I. Matsumoto, K. Ishibashi, S. Sasaki, K. Abe, Aquaporin-11 knockout mice and polycystic kidney disease animals share a common mechanism of cyst formation, FASEB J. 22 (2008) 3672–3684.
[13] T. Saito, Y. Tanaka, Y. Morishita, K. Ishibashi, Proteomic analysis of AQP11-null kidney: proximal tubular type polycystic kidney disease, Biochem. Biophys. Rep. 13 (2017) 17–21.
[14] E.N. Atochina-Vasserman, A. Biktasova, E. Abramova, D.S. Cheng, V.V. Polosukhin, H. Tanjore, S. Takahashi, H. Sonoda, L. Foye, C. Venkov, S.V. Ryzhov, S. Novitskiy, N. Shlonimskaya, M. Ikeda, T.S. Blackwell, W.E. Lawson, A.J. Gow, R.C. Harris, M.M. Dikov, E.E. Tchekneva, Aquaporin 11 insufficiency modulates kidney susceptibility to oxidative stress, Am. J. Physiol. Ren. Physiol. 304 (2013) 1295–1307.
[15] K. Bedard, K.H. Krause, The NOX family of ROS-generating NADPH oxidases: physiology and pathophysiology, Physiol. Rev. 87 (2007) 245–313.
[16] M. Redza-Dutordoir, D.A. Averill-Bates, Activation of apoptosis signaling pathways by reactive oxygen species, Biochim. Biophys. Acta 1863 (2016) 2977–2992.
[17] R.L. Maser, D. Vassmer, B.S. Magenheimer, J.P. Calvet, Oxidant stress and reduced antioxidant enzyme protection in polycystic kidney disease, J. Am. Soc. Nephrol. 13 (2002) 991–999.
[18] V. Menon, D. Rudym, P. Chandra, D. Miskulin, R. Perrone, M. Sarnak, Inflammation, oxidative stress, and insulin resistance in polycystic kidney disease, Clin. J. Am. Soc. Nephrol. 6 (2011) 7–13.
[19] M. Zeier, P. Fehrenbach, S. Geberth, K. Möhring, R. Waldherr, E. Ritz, Renal histology in polycystic kidney disease with incipient and advanced renal failure, Kidney Int. 42 (1992) 1259–1265.
[20] D. Zheng, M. Wolfe, B.D. Cowley Jr, D.P. Wallace, T. Yamaguchi, J.J. Grantham, Urinary excretion of monocyte chemoattractant protein-1 in autosomal dominant polycystic kidney disease, J. Am. Soc. Nephrol. 14 (2003) 2588–2595.
[21] A. Karihaloo, F. Koraishy, S.C. Huen, Y. Lee, D. Merrick, M.J. Caplan, S. Somlo, L.G. Cantley, Macrophages promote cyst growth in polycystic kidney disease, J. Am. Soc. Nephrol. 22 (2011) 1809–1814.
[22] B. Hocher, C. Thöne-Reineke, P. Rohmeiss, F. Schmager, T. Slowinski, V. Burst, F. Siegmund, T. Quertermous, C. Bauer, H.H. Neumayer, W.D. Schleuning, F. Theuring, Endothelin-1 transgenic mice develop glomerulosclerosis, interstitial fibrosis, and renal cysts but not hypertension, J. Clin. Investig. 99 (1997) 1380–1389.
[23] T. Shindo, H. Kurihara, K. Maemura, Y. Kurihara, O. Ueda, H. Suzuki, T. Kuwaki, K.H. Ju, Y. Wang, A. Ebihara, H. Nishimatsu, N. Moriyama, M. Fukuda, Y. Akimoto, H. Hirano, H. Morita, M. Kumada, Y. Yazaki, R. Nagai, K. Kimura, Renal damage and salt-dependent hypertension in aged transgenic mice overexpressing endothelin-1, J. Mol. Med. 80 (2002) 105–116.
[24] T. Nakamura, I. Ebihara, M. Fukui, S. Osada, Y. Tomino, T. Masaki, K. Goto, Y. Furuichi, H. Koide, Increased endothelin and endothelin receptor mRNA expression in polycystic kidneys of cpk mice, J. Am. Soc. Nephrol. 4 (1993) 1064–1072.
[25] A.C. Ong, L.J. Newby, M.R. Dashwood, Expression and cellular localisation of renal endothelin-1 and endothelin receptor subtypes in autosomal-dominant polycystic kidney disease, Nephron Exp. Nephrol. 93 (2003) 80–86.
[26] D.P. Choma, R. Vanacore, H. Naylor, I.A. Zimmerman, A. Pavlichenko, A. Pavlichenko, L. Foye, D.P. Carbone, R.C. Harris, M.M. Dikov, E.E. Tchekneva, Aquaporin 11 variant associates with kidney disease in type 2 diabetic patients, Am. J. Physiol. Ren. Physiol. 310 (2016) 416–425.
[27] J.I. Park, S.H. Yang, J.P. Lee, S.H. Yoo, Y.S. Kim, Genetic predisposition of donors affects the allograft outcome in kidney transplantation: single-nucleotide polymorphism of aquaporin-11, Kidney Res. Clin. Pract. 34 (2015) 47–52.
[28] Y.H. You, S. Okada, S. Ly, K. Jandeleit-Dahm, D. Barit, T. Namikoshi, K. Sharma, Role of Nox2 in diabetic kidney disease, Am. J. Physiol. Ren. Physiol. 304 (2013) 840–848.
[29] A. Djamali, A. Vidyasagar, M. Adulla, D. Hullett, S. Reese, Nox-2 is a modulator of fibrogenesis in kidney allografts, Am. J. Transplant. 9 (2009) 74–82.
[30] M.F. Cesta, Normal structure, function, and histology of the spleen, Toxicol. Pathol. 34 (2006) 455–465.